HOKKAIDO UNIVERSITY

Title	Two-dimensional observations of midlatitude sporadic E irregularities with a dense GPS array in Japan
Author(s)	Maeda, Jun; Heki, Kosuke
Citation	Radio Science, 49(1), 28-35 https://doi.org/10.1002/2013RS005295
Issue Date	2014-01
Doc URL	http://hdl.handle.net/2115/57020
Rights	Copyright 2014 American Geophysical Union.
Type	article
File Information	RadSci_49_28-.pdf

Instructions for use

Two-dimensional observations of midlatitude sporadic E irregularities with a dense GPS array in Japan

Jun Maeda[1] and Kosuke Heki[1]

[1]   We observed two-dimensional structure and time evolution of ionospheric irregularities caused by midlatitude sporadic E (E_s) over Japan as positive anomalies of total electron content (TEC) by analyzing the data from the nationwide Global Positioning System (GPS) array. In this paper we report a case study of strong E_s observed in the local evening of 21 May 2010, over Tokyo, Japan. In the slant TEC time series, E_s showed a characteristic pulse-like enhancement of ~1.5 TEC units lasting for ~10 min. We plotted these positive TEC anomalies on the subionospheric points of station-satellite pairs to study the horizontal structure of the E_s irregularity. We confirmed that the irregularity existed at the height of ~106 km by comparing the data of multiple GPS satellites, which is consistent with the local ionosonde observations. The horizontal shapes of the E_s irregularity showed frontal structures elongated in E-W, spanning ~150 km in length and ~30 km in width, composed of small patches. The frontal structure appears to consist of at least two parts propagating in different directions: one moved eastward by ~60 m s^{-1}, and the other moved southwestward by ~80 m s^{-1}. Similar TEC signatures of E_s were detected by other GPS satellites, except one satellite that had line of sight in the N-S direction which dips by 40–50° toward north, which indicates the direction of plasma transportation responsible for the E_s formation. We also present a few additional observation results of strong E_s irregularities.

1.   Introduction

[2]   Sporadic E (E_s) is a thin layer appearing occasionally at altitudes of ~100 km in the ionospheric E region. It is characterized by anomalously high electron densities that often exceed those in the F region high above (~300 km). It often causes irregular propagation of high frequency and very high frequency radio waves. It also causes scintillations in microwaves, degrading the accuracy of Global Navigation Satellite System (GNSS), including Global Positioning System (GPS).

[3]   Although midlatitude E_s has been studied for over half a century [*Whitehead*, 1989; *Mathews*, 1998], there have been few examples of its direct imaging. Because ground-based radars such as ionosondes, over-the-horizon radars, coherent and incoherent scatter radars, including the middle and upper atmosphere radar, have limited spatial and temporal coverage, it has been difficult to capture the whole horizontal structure of E_s. Nevertheless, these radars, together with conventional ionosondes, have found that E_s irregularities have horizontally patchy structures [*Whitehead*, 1972; *Miller and Smith*, 1975, 1978].

[4]   *Maruyama* [1991, 1995] used a geostationary satellite to study the dynamics of the midlatitude E_s by examining quasi-periodic scintillations on 136 MHz and inferred its elongated shape. *Yamamoto et al.* [1991] found quasiperiodic echoes from the lower region of the ionosphere, which enabled *Yamamoto et al.* [1998] to infer the E_s structure indirectly. In recent years, there have been intensive rocket experiments of E_s combined with ground-based observations [*Larsen et al.*, 1998, 2005; *Wakabayashi et al.*, 2005; *Yamamoto et al.*, 2005] along with numerical experiments [e.g., *Yokoyama et al.*, 2005]. As the pioneer work of E_s imaging, *Kurihara et al.* [2010] showed NW-SE aligned patchy structures of Mg$^+$ ions in the E_s layer in southwestern Japan, with a horizontal scale of ~30 km × ~10 km by observations made with a magnesium ion imager on board a rocket.

[5]   In recent years, the GPS radio occultation technique with receivers on board low Earth orbiters has been successful in providing electron density profiles of E_s around the globe. The profiles often detected E_s signatures and helped us investigate diurnal [*Arras et al.*, 2009] and seasonal [*Garcia-Fernandez and Tsuda*, 2006] changes of the global distribution of E_s. However, the horizontal resolution of GPS radio occultation data is not sufficient to image individual E_s patches, and temporal resolution of this technique is not high enough either.

[6]   In our study, we show the usefulness of a method to image E_s irregularities by measuring the number of electrons along the paths connecting densely deployed ground-based receivers and GPS satellites. Although the original purpose

---

[1]Department of Natural History Sciences, Hokkaido University, Sapporo, Japan.

Corresponding author: J. Maeda, Department of Natural History Sciences, Hokkaido University, N10 W8, Kita-ku, Sapporo, Hokkaido 060-0810, Japan. (jun.maeda@mail.sci.hokudai.ac.jp)
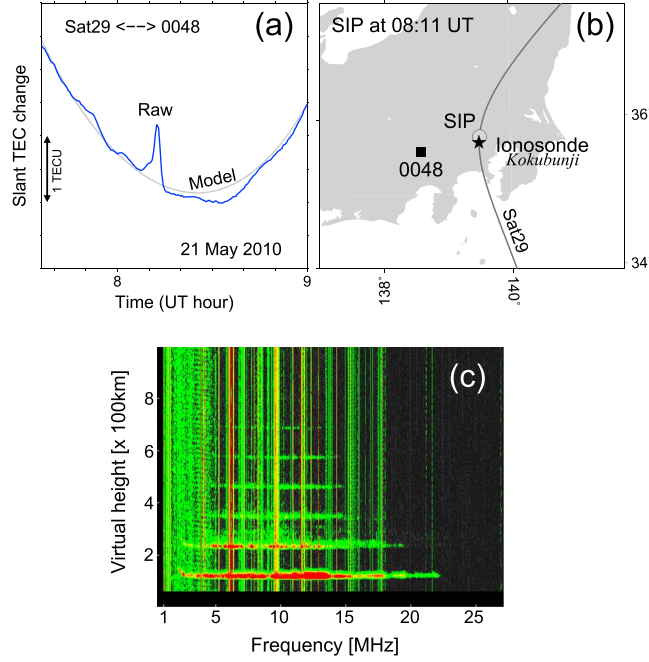
Figure 1. Time series of slant TEC observed at 0048 using Satellite 29 (blue curve) showing E_s signature around 08:10–08:15 UT as a short positive TEC anomaly of ~1 TECU. (a) The model curve was drawn by modeling the vertical TEC change using a cubic polynomial of time (see *Ozeki and Heki* [2010] for the detail). (b) The SIP track passes through the Kokubunji ionosonde station at ~08:11 UT. (c) The 08:15 UT ionogram at Kokubunji observed the highest foE_s of ~22 MHz.

of the GPS network is to measure crustal deformations, it can be also used to measure ionospheric total electron content (TEC), the number of electrons integrated along the line of sight (LOS). This method, often called GPS-TEC, has been widely used for detecting traveling ionospheric disturbances (TIDs) [*Saito et al.*, 2002; *Tsugawa et al.*, 2004; *Hayashi et al.*, 2010], spread *F* [*Mendillo et al.*, 2001], and ionospheric disturbances by earthquakes [*Heki and Ping*, 2005; *Astafyeva et al.*, 2009] and volcanic eruptions [*Heki*, 2006].

[7] To study the two-dimensional structure and time evolution of E_s, we used GEONET (GNSS Earth Observation Network), a dense array of permanent GPS stations composed of ~1200 stations throughout Japan operated by GSI (Geospatial Information Authority of Japan). Its high spatial density (typical horizontal separations are 15–25 km) and time resolution (regularly sampled every 30 s) would make it an ideal tool to image the horizontal structure and temporal evolution of E_s irregularities in detail.

2. Method

[8] GPS satellites transmit microwave signals with two carrier frequencies, namely, ~1.5 GHz (L1) and ~1.2 GHz (L2). GPS receiving stations of GEONET record the phase of these carriers every 30 s, and the raw data are available online (terras.gsi.go.jp). The ionospheric delay is inversely proportional to the square of the frequency as the first approximation [*Kedar et al.*, 2003], and the temporal change of the phase difference between the two carrier waves expressed in length, often called L4 (L4 $\equiv$ L1 $-$ L2), is proportional to the change in TEC along the LOS (slant TEC). Slant TEC time series show U-shaped curves as the incident angle of LOS in

the ionosphere changes as the satellite moves in the sky. Without strong ionospheric disturbances, such as occurrences of solar flares and passages of traveling ionospheric disturbances, slant TEC changes smoothly in time.

[9] To compare GPS-TEC with ground-based sensors, we used ionosonde data to obtain foE_s (the critical frequency of E_s) and $h'E_s$ (the height of E_s) at the Kokubunji observatory, Tokyo, of the National Institute of Information and Communications Technology (NICT) (black star in Figure 1b). Ionosonde data are available online at wdc.nict.go.jp/IONO/. We first searched for the occurrences of strong E_s with foE_s exceeding 20 MHz in the ionosonde data. Then we downloaded raw GPS data files on the E_s occurrence days and converted them into TEC time series to study E_s signatures.

[10] E_s irregularities are recognized as pulse-like TEC increases in slant TEC time series. The blue curve in Figure 1a shows the typical E_s signature in the slant TEC observed at a GPS station in central Japan on 21 May 2010, using Satellite 29. Here we assumed that the vertical TEC changes in time as a cubic polynomial of time t (model shown in Figure 1a as a smooth gray curve). The detail of the model fitting procedure is given in *Ozeki and Heki* [2010]. The vertical TEC anomalies shown in Figures 3 and 4 were derived by multiplying the residual slant TEC with the cosine of the incident angle of LOS with a thin layer at the E_s altitude.

3. Results

3.1. E_s Signature in Slant TEC

[11] The typical E_s signature in slant TEC (blue curve in Figure 1a) appears at around 08:11 UT (17:11 LT) as a
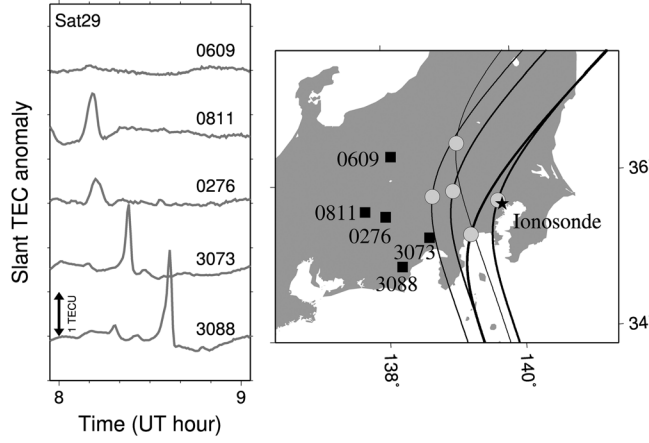
Figure 2. (left) Time series of slant TEC anomalies derived from five different GPS stations in central Japan. (right) Their locations (black squares) and SIP tracks with light gray circles indicating the SIP positions when pulse-like TEC enhancements were recorded. Four out of five GPS stations (i.e., all except 0609) recorded positive TEC pulses. Such highly localized TEC enhancements are peculiar to E_s signatures. The highest positive TEC anomaly was recorded by 3088 at southwest of the ionosonde, counting ~2.0 TECU.

relatively sharp positive pulse of ~1 TECU (TEC unit, 1 TECU = 10^{16} el m^{-2}) lasting for ~10 min. At this time, the LOS is considered to have passed through one of the E_s patches of very high electron density. Almost at the same time (08:15 UT), the Kokubunji ionosonde station recorded a strong E_s with the maximum foE_s of 22 MHz (Figure 1c). We calculated the positions of ionospheric penetration point (IPP) of LOS assuming the height of 106 km, referring to

$h'E_s$ observed at the ionosonde. The subionospheric point (SIP), the ground projection of IPP, is close to the ionosonde (Figure 1b), suggesting that the ionosonde and GPS-TEC detected the same patch of E_s.

[12] In Figure 2, the slant TEC anomalies observed at five different GPS stations are shown. Four of them show positive TEC anomalies, including the one with an SIP near the ionosonde (3073). The GPS stations with pulse-like anomalies
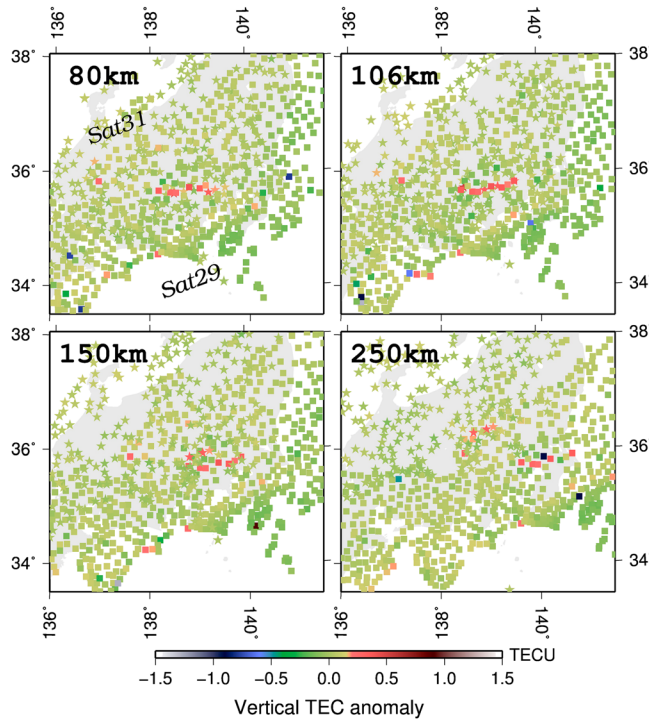

Figure 3. VTEC anomaly maps drawn assuming different heights of IPP using the two satellites (square: 29, star: 31) at 08:00 UT on 21 May 2010. With the IPP height of 106 km, positive anomalies elongated in E-W by the two satellites coincide with each other. This height is also consistent with the $h'E_s$ at Kokubunji (Figure 1c).
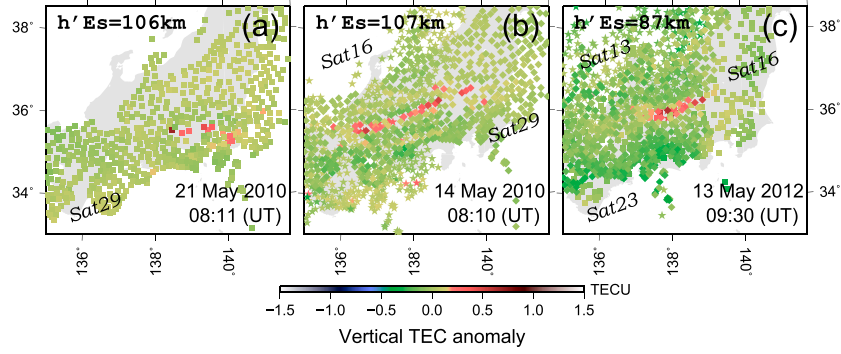
3

Figure 4. Vertical TEC anomaly map at 08:11 UT on (a) 21 May 2010 with Satellite 29 and those on (b) 14 May 2010 and (c) 13 May 2012. The IPP height is determined by referring $h'E_s$ observed at the Kokubunji ionosonde. In all cases, foE_s exceeding 20 MHz were observed by the ionosonde. Typical E-W or ENE-WSW frontal structures, spanning 100–350 km, can be seen.

line up in E-W. Station 0609, off this line, does not show such anomaly. Such highly localized nature of the TEC anomaly is peculiar to E_s and rules out other possibilities such as TIDs and solar flares. TIDs would have much larger spatial scales and longer periods, and solar flares would have left similar signatures over the whole sunlit hemisphere (there were no reports of a solar flare at this time). Thus, we consider this a signature of E_s.

3.2. Altitude of the E_s Signature in TEC

[13] In Figure 3, we mapped the vertical TEC (VTEC) anomalies at 08:00 UT using two different satellites. There we assume four different IPP heights in order to constrain the altitude of the anomalies. The IPP height of 80 km corresponds to the D region of the ionosphere; and 106 km, 150 km, and 280 km correspond to the E region and the F_1 and F_2 layers, respectively. In assuming the IPP height for
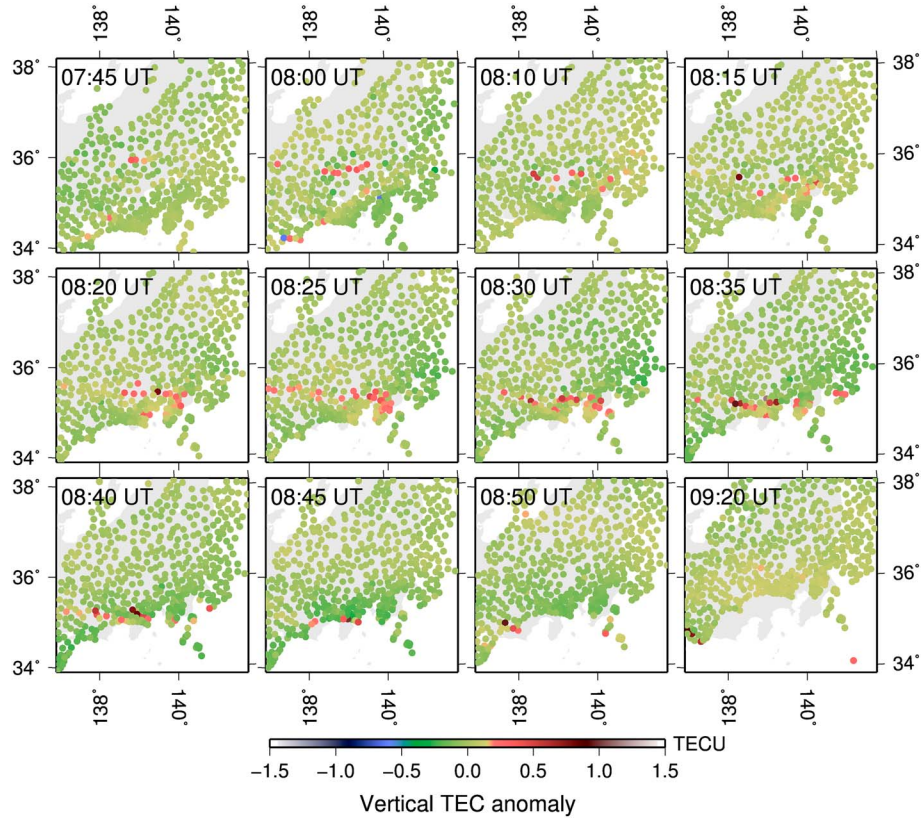

Figure 5. Snapshots of VTEC anomaly maps at various time epochs from 07:45 UT to 09:20 UT on 21 May 2010. The movement of the E_s patches can be seen. The shape and the direction of the E_s patches seem to have switched around 08:25 UT. Before that time, the E_s patches showed a frontal structure elongated in E-W and moved eastward. After that time, the frontal structure fragmented into smaller patches that aligned in NW-SE and moved southwestward.
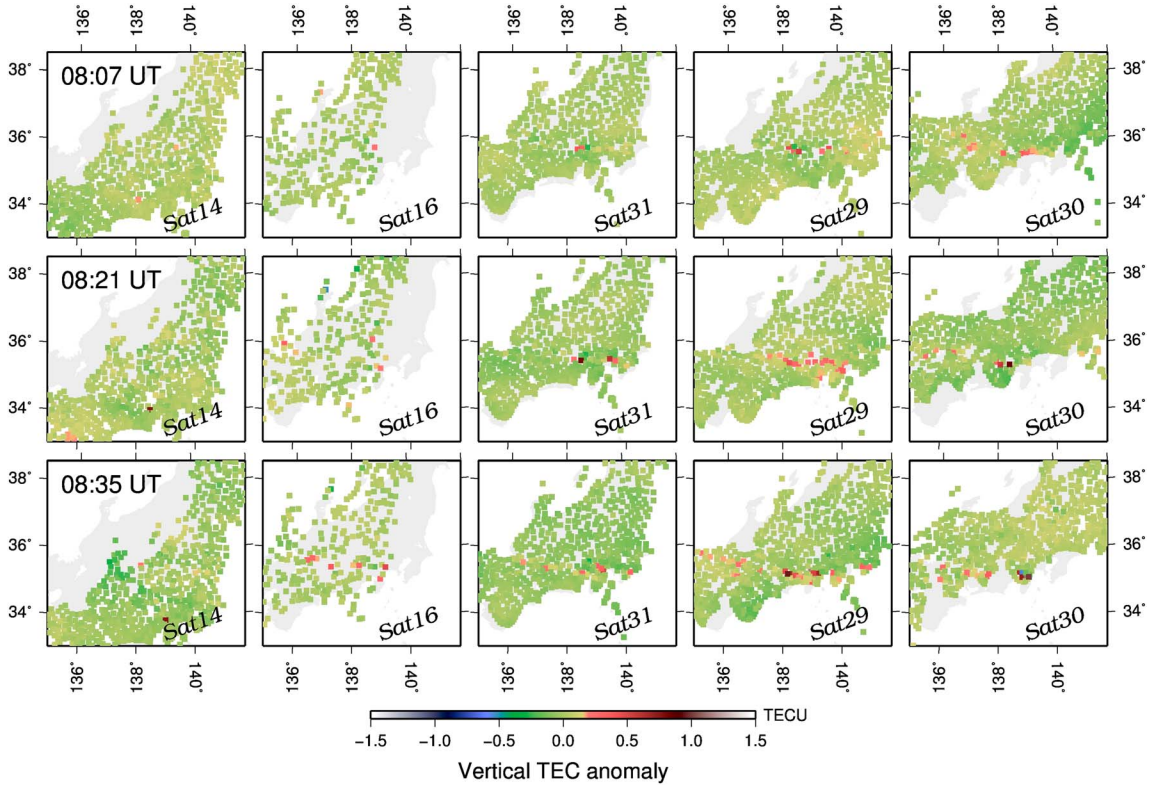
4

Figure 6. The VTEC anomaly maps at 08:07 UT, 08:21 UT, and 08:35 UT derived from five different satellites. Data from Satellite 16 are sparsely distributed because of the data loss due to low elevation angles. The E_s structure appears somewhat different among the satellites, suggesting small-scale patchy structures of high electron densities. Satellite 14 could not capture the E_s irregularities during this period, which suggests that the plasma transportation responsible for the E_s formation occurred along the LOS of this satellite.

the E region, we adopted the value of $h'E_s$ observed at the Kokubunji ionosonde.

[14] In Figure 3, among the majority of SIPs of green color indicating no anomalies, there are some red and blue points indicating positive and negative anomalies, respectively. The positive anomaly (red dots) at 08:00 UT observed with Satellite 29 and Satellite 31 shows simple linear structures running E-W, an ideal situation to make it possible to constrain the height of this linear anomaly. With the IPP height of 106 km, two linear structures obtained from the two satellites coincide, while gaps emerge with higher and lower IPP heights. Considering that the $h'E_s$ at Kokubunji ionosonde was 106 km, we conclude confidently that the observed TEC anomalies are the signature of irregularities at the E region of the ionosphere.

3.3. Horizontal Structure

[15] Figure 4a shows the snapshot of VTEC anomalies at 08:11 UT around central Japan drawn with the IPP height of 106 km. Since the distances between GEONET stations are 15–25 km, the spatial resolution of the VTEC anomaly maps is approximately ~25 km. Figure 4a shows that the E_s irregularity has a frontal structure elongated in E-W with the dimension of ~150 km in E-W and ~30 km in N-S.

[16] Similar structures have been observed for strong E_s irregularities (whose foE_s are over 20 MHz) that occurred on other days, i.e., 14 May 2010 (Figure 4b) and 13 May 2012 (Figure 4c). There we can see similar frontal structures running

roughly ENE-WSW. These anomalies have been also confirmed to be E_s by constraining the anomaly altitudes in the same way as described in section 3.2, i.e., comparison of VTEC anomaly maps from two satellites and $h'E_s$ from ionosonde. The lengths of the positive anomalies are ~350 km for the case of 14 May 2010 and ~150 km for the other two cases. This would be the first successful imaging of the whole E_s irregularity with a large-scale E-W frontal structure.

3.4. Horizontal Movement

[17] Next we have a look at the VTEC anomalies on 21 May 2010, at various time epochs (Figure 5), and study the time evolution of the horizontal structure of the E_s irregularity. The frontal structures are clearly seen at 08:00, 08:10, and 08:20 UT. The E_s patches line up in ENE-WSW at 08:00 UT and in E-W during 08:10–08:20 UT. In the snapshots after 08:25 UT, the characteristic E-W frontal structure seems to have dissolved into smaller patches of a size of ~80 km with a weak alignment in WNW-ESE. These snapshots suggest that the lifetime of this frontal structure of E_s irregularities was not much longer than a few tens of minutes.

[18] The movement of the regions with positive TEC anomalies was first eastward before 08:25 UT when the characteristic E-W frontal shape is intermittently seen. The approximate speed of its motion is assumed to be ~60 m s^{-1} by measuring the distance between the SIPs of the eastern edges of the E-W structure at 08:00 UT and 08:15 UT. After 08:25 UT, the E-W frontal structure broke into smaller

patches and moved southwestward at the speed of ~80 m s^{-1}. These southwestward movements of NW-SE aligned patches are typically seen at 08:35, 08:40, and 08:50 UT. Thus, there seems to be at least two patches that consist of the E-W frontal structure, i.e., patches moved eastward and southwestward. This is also supported by the shapes of the positive TEC pulses in the time series of slant TEC anomalies (Figure 2). There, the shapes of TEC pulses recorded at 0811 and 0276 are considerably different from those at 3073 and 3088, i.e., the peaks of the former pairs are longer and smaller than those of the latter pairs. The former and latter pairs represent the TEC anomalies caused by the patch that moved eastward and southwestward, respectively. Hence, combined analysis of VTEC anomaly maps and slant TEC time series can reveal the hidden patch movements in a large-scale E_s structure.

3.5. Direction of Plasma Transportation

[19] Figure 6 shows the VTEC anomaly maps at 08:07 UT, 08:21 UT, and 08:35 UT derived from five different GPS satellites available during the period of the E_s appearance. It is noteworthy that only Satellite 14, among the five satellites, failed to detect the E-W frontal structure of E_s in the period 08:07–08:35 UT. Although the ionosonde at Kokubunji detected the strong E_s at 08:15 UT and 08:30 UT, Satellite 14 does not show positive TEC anomalies anywhere in the entire network, including the station with an SIP close to the ionosonde. Such a lack of the E_s signature may reflect the direction of plasma transportation responsible for the E_s formation. Since TEC corresponds to the integrated number of electrons along the LOS, no anomaly would be seen if the plasmas have moved along the LOS. In this case, plasmas might have been transported in the direction close to the Satellite 14 LOS, that is, nearly N-S in azimuth with the dip of 40–50° toward north. This suggests that the transportation may have occurred along the local geomagnetic field direction, but further studies are necessary to find out if this is a general phenomenon.

4. Discussion

[20] We showed several examples of E_s observations with GPS-TEC. The three most important points we have shown are the following: (1) the horizontal shapes and dimension of E_s patches, (2) the horizontal velocities of E_s patches, and (3) the direction of plasma transportation responsible for E_s formation. Here we discuss these points as well as the advantages and limitations of E_s observations with GPS-TEC.

4.1. Horizontally Patchy Structures of E_s

[21] In Figure 6, we can see that the same E_s irregularity looks fairly different when viewed with different satellites. Satellite 29 provides the clearest image of the whole horizontal structure of the E_s irregularity. The temporal evolution of its horizontal structure also looks fairly different with different satellites. For example, Satellite 16 captured the E-W frontal structure at later time epochs, e.g., at 08:35 UT. On the other hand, Satellite 31 seems to have lost sight of the E-W frontal structure after 08:21 UT. Such satellite-dependent images of the E_s structure seem to reflect its complicated three-dimensional patchy structure. The Kokubunji ionogram at 08:15 UT (Figure 1c) shows "blanket E_s," i.e., the highly ionized E_s layer makes a continuous flat plane, which seems

inconsistent with the highly patchy structure suggested by the GPS-TEC observations. We consider that such patches may correspond to regions with very high electron density (i.e., $foE_s > 20$ MHz) for which only GPS-TEC observations are sensitive.

4.2. Estimation of the Thickness of the E_s Layer

[22] Here we estimate the thickness of the E_s layer by comparing the electron density inferred from critical frequency observations of the ionosonde with the amplitude of the positive TEC anomaly from GPS-TEC observations. For the E_s irregularity in Figure 1, the peak foE_s was ~20 MHz at 08:15 UT (Figure 1c). This corresponds to the peak plasma density of 5.0×10^{12} el m^{-3} according to the equation in *Reddy and Rao* [1968], i.e.,

$$fo \approx 8.98 \times \sqrt{N_e}$$

where fo is the critical frequency (Hz), and N_e is the electron density (el m^{-3}). As the TEC enhancement above the ionosonde was approximately ~1 TECU (1.0×10^{16} el m^{-2}), the thickness of the E_s layer is estimated as ~2 km. This is consistent with earlier reports by GPS radio occultation observations [*Garcia-Fernandez and Tsuda*, 2006] and rocket experiments [*Wakabayashi and Ono*, 2005].

4.3. Dynamics of E_s Irregularities

[23] Figures 2 and 5 show that E_s patches moved in different directions and speeds. When an E-W frontal structure was clearly seen, the individual patches that consist the frontal structure moved eastward at ~60 m s^{-1}. After the dissipation of the E-W frontal structure, at least two smaller band-like patches that aligned in NW-SE appeared and propagated southwestward at ~80 m s^{-1} (typically seen in the snapshots at 08:35 and 08:40 UT in Figure 5). This result indicates that different mechanisms may have worked in the eastward movements in the large E-W frontal structure and in the southwestward movements of smaller E_s patches.

[24] Zonal wind profiles were obtained from the SEEK (Sporadic-E Experiment over Kyushu) experiment [*Larsen et al.*, 1998], and the present result of the eastward speed is almost consistent with their results. *Whitehead* [1989] pointed out that E_s tends to drift eastward, especially during daytime, and this is consistent with the general tendency of the neutral wind direction in the ionospheric E region [*Kolawole and Derblom*, 1978; *Tanaka*, 1979]. Although the neutral wind data are not available for the E_s studied here, it may be possible to estimate the approximate neutral wind velocity from the velocity of these E_s patches.

[25] On the southwestward movements of NW-SE aligned smaller band structures, previous studies have reported the preference of such alignment azimuth and propagation direction of midlatitude E_s in the Northern Hemisphere [*Tsunoda and Cosgrove*, 2001; *Cosgrove and Tsunoda*, 2002; *Tsunoda et al.*, 2004]. In the snapshot of a VTEC map at 08:35 UT and 08:40 UT in Figure 5, we can see a wavelike structure consisting of two individual E_s bands. The bands are horizontally separated by 30–40 km, which is consistent with the wavelength of gravity waves observed at an altitude of 100 km in this region. *Cosgrove* [2007] have pointed out that the polarization electric field modulated by gravity waves at the F region can modulate the E region background plasma

through the electrodynamical coupling. This suggests that the observed southwestward movements of NW-SE aligned E_s irregularities might be driven by the atmospheric gravity waves.

[26] In the midlatitude region of the Northern Hemisphere, medium-scale traveling ionospheric disturbances (MSTIDs) often appear at night and propagate southwestward [*Saito et al.*, 2002]. Considering the electrodynamical coupling between the *F* and *E* regions of the ionosphere, *Tsunoda and Cosgrove* [2001] suggested the influence of TIDs on E_s generation in the nighttime midlatitude ionosphere. *Bowman* [1960, 1968] pointed out that an E_s band is often accompanied with a TID, and this was true in 11 cases out of 13 (85%). For all the cases shown in Figure 4, we did not find simultaneous MSTID activities with GPS-TEC analysis, although we found that MSTIDs followed E_s activities 0.5 and 3 h later for the cases in Figures 4a and 4c, respectively. The wavefronts of both MSTIDs are typically aligned in NW-SE and propagated southwestward. Since MSTIDs frequently appear at night in this region, it is not clear if the E_s and the subsequent MSTID had any causal relationships. Because GPS-TEC can observe both E_s and MSTID, we could perform statistical studies on evening-type E_s irregularities in the future in order to examine the electrodynamic coupling between E_s and MSTIDs.

4.4. GPS-TEC: Advantages and Limitations on E_s Observations

[27] One of the advantages of GPS-TEC over conventional radar observations is its high spatial (25 km) and temporal (30 s) resolution. This technique is useful to detect relatively large E_s irregularities with spatial scale of a few hundreds of kilometers as well as small E_s patches of a few tens of kilometers. It is also important to note that the 30 s time resolution of GPS-TEC is useful to study their dynamics. By using several satellites to cover the large geographical distance and time width, GPS-TEC can capture the whole process of E_s formation and decay.

[28] Another merit is that the direction of plasma transportation can be inferred. As shown in Figure 6, by comparing E_s signatures among different GPS satellites, the plasma transportation responsible for the E_s formation is estimated to have occurred in the N-S direction which dips by 40–50° toward north. According to the wind shear theory, the $\mathbf{V} \times \mathbf{B}$ forces let positive metallic ions condense into a thin layer in the presence of vertical wind shear [*Whitehead*, 1960, 1970, 1989]. Our result shows that GPS-TEC can be used to infer the plasma movements that contribute to the E_s formation. Owing to the spatial density of ground GPS stations and the availability of multiple satellites in the sky, GPS-TEC has a strong potential of investigating the dynamics of formation and decay of E_s irregularities through three-dimensional observations of the plasma movements.

[29] One of the limitations of the GPS-TEC technique on E_s observations would be that we can see only strong E_s, say, with foE_s more than ~20 MHz. Because the background TEC is dominated by the electrons in the *F* region, even small scintillation in the *F* region can mask the E_s signatures in TEC time series. While a number of observations and theoretical models suggest that the E_s layer is modulated in altitude [*Woodman et al.*, 1991; *Larsen*, 2000; *Bernhardt*, 2002; *Cosgrove and Tsunoda*, 2002; *Yokoyama et al.*, 2009], the GPS-TEC technique is not good at detecting such small-scale vertical structures of E_s irregularities, which may potentially be another limitation.

[30] In Figure 3, we demonstrated that the E_s height could be constrained by the GPS-TEC technique by matching the frontal structure of the E_s irregularity by multiple satellites. The height resolution depends on the incident angles of the LOS to the E_s layer, i.e., lower incident angles give higher height resolution. In the case of Figure 3, the incident angles are ~70° for Satellite 31 and ~45° for Satellite 29. In that case, the height resolution was ~20 km, i.e., changing the E_s height by this amount results in significant inconsistency of the ground projections of E_s from the two satellites. In other words, GPS-TEC itself could distinguish the E_s layer at an altitude of 100 km from the *D* (80 km), F_1 (150 km), and F_2 layers (250 km) without relying on ionosonde observations. This suggests the possibility of automatic detection of E_s by GPS-TEC in the future.

[31] Further densification of the GEONET data in space will be realized by incorporating data from GNSS (Global Navigation Satellite System) other than GPS, which is under progress now by GSI by replacing receivers to new models compatible with multiple GNSS. Hybrid observations by GPS-TEC combined with the radio tomography technique [e.g., *Bernhardt et al.*, 2005] or rocket experiments [e.g., *Kurihara et al.*, 2010] would further improve the spatial resolution of 3-D images of E_s irregularities.

5. Conclusions

[32] In this paper we have presented the first results of two-dimensional observations of the horizontal structure of mid-latitude E_s irregularities with a dense GPS array in Japan and demonstrated that GPS-TEC is a promising technique to study E_s. The results can be summarized as follows.

[33] 1. Strong E_s with foE_s over 20 MHz appears in the slant TEC time series as a pulse-like positive TEC enhancement (~1.5 TECU).

[34] 2. In the VTEC anomaly maps, E_s often shows large-scale frontal structures elongated in the E-W direction and spanning more than 100 km.

[35] 3. We also observed the fragmentation of the E-W frontal structure into smaller patches and its migration.

[36] 4. Observations with multiple satellites suggested that the E-W frontal structure is composed of small patches with very high electron density and that the plasma transportation responsible for the E_s formation occurred in a direction close to the local geomagnetic field in the case of 21 May 2010.

References

Arras, C., C. Jaobi, and J. Wickhert (2009), Semidiurnal tidal signature in sporadic E occurrence rates derived from GPS radio occultation measurements at higher midlatitudes, *Ann. Geophys.*, 27, 2555–2563, doi:10.5194/angeo-27-2555-2009.

Astafyeva, E., K. Heki, V. Kiryushkin, E. Afraimovich, and S. Shalimov (2009), Two-mode long-distance propagation of coseismic ionosphere disturbances, *J. Geophys. Res.*, 114, A10307, doi:10.1029/2008JA013853.

Bernhardt, P. A. (2002), The modulation of sporadic-E layers by Kelvin-Helmholtz billows in the neutral atmosphere, *J. Atmos. Sol. Terr. Phys.*, 64, 1487–1504.

Bernhardt, P. A., et al. (2005), Radio tomographic imaging of sporadic-E layers during SEEK-2, *Ann. Geophys.*, 23, 2357–2368.

Bowman, G. G. (1960), Some aspects of sporadic *E* at mid-latitudes, *Planet. Space Sci.*, *2*, 195.

Bowman, G. G. (1968), Movements of ionospheric irregularities and gravity waves, *J. Atmos. Terr. Phys.*, *630*, 721.

Cosgrove, R. B. (2007), Wavelength dependence of the linear growth rate of the E_s layer instability, *Ann. Geophys.*, *25*, 1311–1322, doi:10.5194/angeo-25-1311-2007.

Cosgrove, R. B., and R. T. Tsunoda (2002), A direction-dependent instability of sporadic-*E* layers in the nighttime midlatitude ionosphere, *Geophys. Res. Lett.*, *29*(18), 1864, doi:10.1029/2002GL014669.

Garcia-Fernandez, M., and T. Tsuda (2006), A global distribution of sporadic *E* events revealed by means of CHAMP-GPS occultations, *Earth Planets Space*, *58*, 33–36.

Hayashi, H., N. Nishitani, T. Ogawa, Y. Otsuka, T. Tsugawa, K. Hosokawa, and A. Saito (2010), Large-scale traveling ionospheric disturbance observed by superDARN Hokkaido HF radar and GPS networks on 15 December 2006, *J. Geophys. Res.*, *115*, A06309, doi:10.1029/2009JA014297.

Heki, K. (2006), Explosion energy of the 2004 eruption of the Asama Volcano, central Japan, inferred from ionospheric disturbances, *Geophys. Res. Lett.*, *33*, L14303, doi:10.1029/2006GL026249.

Heki, K., and J.-S. Ping (2005), Directivity and apparent velocity of the coseismic ionospheric disturbances observed with a dense GPS array, *Earth Planet. Sci. Lett.*, *236*, 845–855.

Kedar, S., G. A. Hajj, B. D. Wilson, and M. B. Heflin (2003), The effect of the second order GPS ionospheric correction on receiver positions, *Geophys. Res. Lett.*, *30*(16), 1829, doi:10.1029/2003GL017639.

Kolawole, L. B., and H. Derblom (1978), Skywave backscatter studies of temperate latitude Es, *J. Atmos. Terr. Phys.*, *40*, 785–792.

Kurihara, J., et al. (2010), Horizontal structure of sporadic *E* layer observed with a rocket-borne magnesium ion imager, *J. Geophys. Res.*, *115*, A12318, doi:10.1029/2009JA014926.

Larsen, M. F. (2000), A shear instability seeding mechanism for quasiperiodic radar echoes, *J. Geophys. Res.*, *105*(A11), 24,931–24,940, doi:10.1029/1999JA000290.

Larsen, M. F., S. Fukao, M. Yamamoto, R. Tsunoda, K. Igarashi, and T. Ono (1998), The SEEK chemical release experiment: Observed neutral wind profile in a region of sporadic-*E*, *Geophys. Res. Lett.*, *25*, 1789–1792.

Larsen, M. F., M. Yamamoto, S. Fukao, and R. T. Tsunoda (2005), SEEK 2: Observations of neutral winds, wind shears, and wave structure during a sporadic *E*/QP event, *Ann. Geophys.*, *23*, 2369–2375.

Maruyama, T. (1991), Observations of quasi-periodic scintillations and their possible relation to the dynamics of E_s plasma blobs, *Radio Sci.*, *26*(3), 691–700, doi:10.1029/91RS00357.

Maruyama, T. (1995), Shapes of irregularities in the sporadic *E* layer producing quasi-periodic scintillations, *Radio Sci.*, *30*(3), 581–590, doi:10.1029/95RS00830.

Mathews, J. D. (1998), Sporadic *E*: Current views and recent progress, *J. Atmos. Sol. Terr. Phys.*, *60*, 413–435.

Mendillo, M., J. Meriwether, and M. Biondi (2001), Testing the thermospheric neutral wind suppression mechanism for day-to-day variability of equatorial spread *F*, *J. Geophys. Res.*, *106*(A3), 3655–3663, doi:10.1029/2000JA000148.

Miller, K. L., and L. G. Smith (1975), Horizontal structure of mid-latitude sporadic *E* layers observed by incoherent scatter radar, *Radio Sci.*, *10*, 271–276.

Miller, K. L., and L. G. Smith (1978), Incoherent scatter radar observations of irregular structure in mid-latitude sporadic *E* layers, *J. Geophys. Res.*, *33*, 3761–3775.

Ozeki, M., and K. Heki (2010), Ionospheric holes made by ballistic missiles from North Korea detected with a Japanese dense GPS array, *J. Geophys. Res.*, *115*, A09314, doi:10.1029/2010JA015531.

Reddy, C. A., and M. M. Rao (1968), On the physical significance of the Es parameters fbEs, fEs, and foEs, *J. Geophys. Res.*, *73*(1), 215–224, doi:10.1029/JA073i001p00215.

Saito, A., M. Nishimura, M. Yamamoto, S. Fukao, T. Tsugawa, Y. Otsuka, S. Miyazaki, and M. C. Kelley (2002), Observations of traveling ionospheric disturbances and 3-m scale irregularities in the nighttime *F*-region ionosphere with the MU radar and a GPS network, *Earth Planets Space*, *54*, 31–44.

Tanaka, T. (1979), Sky-wave backscatter observations of sporadic-E over Japan, *J. Atmos. Terr. Phys.*, *41*, 203–215.

Tsugawa, T., A. Saito, and Y. Otsuka (2004), A statistical study of large-scale traveling ionospheric disturbances using the GPS network in Japan, *J. Geophys. Res.*, *109*, A06302, doi:10.1029/2003JA010302.

Tsunoda, R. T., and R. B. Cosgrove (2001), Coupled electrodynamics in the nighttime midlatitude ionosphere, *Geophys. Res. Lett.*, *28*, 4171–4174.

Tsunoda, R. T., R. B. Cosgrove, and T. Ogawa (2004), Azimuth-dependent E_s layer instability: A missing link found, *J. Geophys. Res.*, *109*, A12303, doi:10.1029/2004JA010597.

Wakabayashi, M., and T. Ono (2005), Multi-layer structure of mid-latitude sporadic-*E* observed during the SEEK-2 campaign, *Ann. Geophys.*, *23*, 2347–2355.

Wakabayashi, M., T. Ono, T. Mori, and P. A. Bernhardt (2005), Electron density and plasma waves measurement in mid-latitude sporadic-*E* layer observed during the SEEK-2 campaign, *Ann. Geophys.*, *23*, 2335–2345.

Whitehead, J. D. (1960), Formation of the sporadic *E* layer in the temperate zones, *Nature*, *188*, 567.

Whitehead, J. D. (1970), Production and prediction of sporadic *E*, *Rev. Geophys. Space Phys.*, *8*, 65–144.

Whitehead, J. D. (1972), The structure of sporadic *E* from a radio experiment, *Radio Sci.*, *7*, 355–358.

Whitehead, J. D. (1989), Recent work on mid-latitude and equatorial sporadic *E*, *J. Atmos. Terr. Phys.*, *51*, 401–424.

Woodman, R. F., M. Yamamoto, and S. Fukao (1991), Gravity wave modulation of gradient drift instabilities in mid-latitude sporadic *E* irregularities, *Geophys. Res. Lett.*, *18*, 1197–1200, doi:10.1029/91GL01159.

Yamamoto, M., S. Fukao, R. F. Woodman, T. Ogawa, T. Tsuda, and K. Kato (1991), Mid-latitude *E*-region field aligned irregularities observed with the MU radar, *J. Geophys. Res.*, *96*, 15,943–15,949.

Yamamoto, M., T. Ono, H. Oya, R. T. Tsunoda, M. F. Larsen, S. Fukao, and M. Yamamoto (1998), Structures in sporadic-*E* observed with an impedance probe during the SEEK campaign: Comparisons with neutral-wind and radar-echo observations, *Geophys. Res. Lett.*, *25*, 1781–1784.

Yamamoto, M., S. Fukao, R. T. Tsunoda, R. Pfaff, and H. Hayakawa (2005), SEEK-2 (Sporadic-E Experiment over Kyushu 2)—Project outline and significance, *Ann. Geophys.*, *23*, 2295–2305.

Yokoyama, T., M. Yamamoto, S. Fukao, T. Takahashi, and M. Tanaka (2005), Numerical simulation of mid-latitude ionospheric *E*-region based on SEEK and SEEK-2 observations, *Ann. Geophys.*, *23*, 2377–2384.

Yokoyama, T., D. L. Hysell, Y. Otsuka, and M. Yamamoto (2009), Three-dimensional simulation of the coupled Perkins and E_s-layer instabilities in the nighttime midlatitude ionosphere, *J. Geophys. Res.*, *114*, A03308, doi:10.1029/2008JA013789.